ELSEVIER International Journal of Mass Spectrometry and Ion Processes 148 (1995) 77–96

High resolution isochronous mass spectrometer for space plasma applications

L. Gubler[a], P. Wurz[a,*], P. Bochsler[a], E. Möbius[b]

[a]*Physikalisches Institut, University of Bern, Sidlerstrasse 5, CH-3012 Bern, Switzerland*
[b]*Institute for the Study of Earth, Oceans and Space, University of New Hampshire, Durham, NH 03824, USA*

Received 8 February 1995; accepted 5 April 1995

Abstract

We have developed a new type of isochronous mass spectrometer of cylindrical geometry. High mass resolving power and high geometric factor are achieved, which significantly exceed current designs in use for the analysis of energetic particles of space plasmas. In combination with an electrostatic energy analyzer the instrument will be used for the measurement of the elemental, isotopic, and molecular composition of space plasmas. We present a theoretical treatment of linear and isochronous mass spectrometers, and numerical simulations of a laboratory prototype built in order to optimize the instrument for mass resolution and detection efficiency. We also discuss experimental results on isotopic and molecular resolving power obtained with the prototype.

Keywords: Isochronous mass spectrometer; Space instrumentation; Time-of-flight mass spectrometer

1. Introduction

Mass spectrometers intended for use on a spacecraft are subject to severe constraints on instrument design concerning volume, weight, power consumption, and long-term maintenance-free operation of the instrument. For many years, the usual choice for determining in situ the composition of low energy space plasmas was the use of magnetic spectrometers. The combination of electrostatic and magnetic fields permits a separation of ions by mass per charge. In recent years, another type of spectrometry was introduced to space instrumentation, the time of flight versus energy (TOF–*E*) technique, which combines a linear time-of-flight mass spectrometer and an energy measurement [1]. Unlike the early instruments, it is now possible to determine charge and mass separately. This is especially important for resolving multiply charged particles in space plasma applications, e.g. to distinguish C^{6+} from He^{2+} in the solar wind, or O^{+} from S^{2+} in the magnetosphere of Jupiter. Linear TOF versus *E* instruments are now well established for space plasma ion composition measurements. They have been successfully flown on several missions [2,3], and valuable new data have been collected, contributing significantly to the understanding of solar and planetary physics [4].

The next important step in instrument

---

* Corresponding author.

SSDI 0168-1176(95)04175-3

improvement was the realization of isochronous TOF mass spectrometers, where the ions travel in a suitably configured electric field. Isochronous TOF instruments make use of a linearly increasing electrostatic field to repel the ions within the TOF section. Mass resolutions $M/\Delta M$ of 100 and more can be reached when the geometry of the electric field is close to ideal. However, realizations of isochronous instruments so far either have approximated the electric field to a limited degree [5] or have made use of a configuration with an incomplete harmonic field combined with a linear TOF section [6]. In this paper, we present a different type of isochronous TOF mass spectrometer which uses a cylindrically symmetric harmonic potential, i.e. an exact realization of the theoretically perfect field. With this instrument, we realized an approach to limit defocusing of ions inside the TOF region, an effect inherent to current instrument designs [6,7]. Thus, high detection sensitivity is achieved. In combination with the high mass resolution the measurement of isotopic abundances in space plasmas becomes feasible. This will open up important avenues in the study of the Sun and will further other geophysical and astrophysical objectives.

2. Basic instrument design

In the following section, we shall discuss in detail and compare the properties of linear TOF instruments and of isochronous TOF instruments. We shall then introduce a new instrument, CYLMAS, which combines these two techniques. The combination of these two techniques even allows identification of isobaric molecules, as will be shown later.

2.1. Linear TOF instruments

TOF–E instruments combine an electrostatic analyzer, a time-of-flight section and a solid state detector. A schematic drawing of such an instrument is shown in Fig. 1. The electrostatic analyzer selects the incoming ions by their energy to charge ratio (E/Q) and serves also as a trap for ultraviolet light. In the TOF section the flight time, τ, of an ion is measured as it passes through a thin entrance foil and is absorbed by the solid state detector

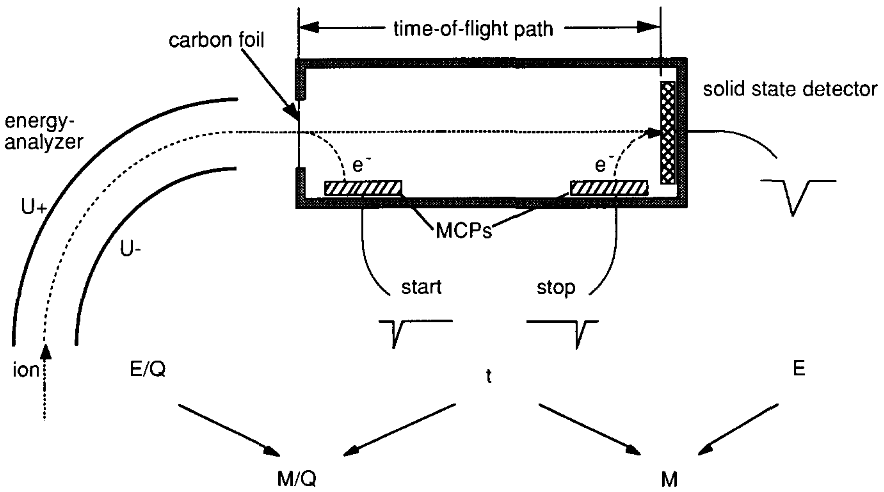

Fig. 1. Schematics of a linear TOF instrument showing the principal elements: entrance system, carbon foil, TOF path, MCP detectors, and the solid state detector.

(SSD) at a distance l away from the entrance foil (Fig. 1). The electron emission from the entrance foil, in most cases made of carbon, provides the start pulse, and the electron emission from the SSD provides the stop pulse for the time measurement. In addition, the SSD determines the residual energy E_{SSD} of the impacting ion. The energy threshold of SSDs makes it necessary to post-accelerate the ions before they enter the TOF–E system. In current instrumentation, post-acceleration voltages (V_a) of 20–30 kV are applied. In such an instrument, the mass per charge M/Q, the mass M, and the charge state Q are given by

$$M/Q = 2(\tau/l)^2\alpha_1(V_a + E/Q)$$

$$M = 2(\tau/l)^2(E_{\mathrm{SSD}}/\alpha_2)$$

$$Q = (E_{\mathrm{SSD}}/\alpha_2)/\left[\alpha_1\left(V_a + \frac{E}{Q}\right)\right]$$

where α_1 describes the energy loss in the foil and α_2 the pulse height defect in SSDs.

This type of TOF, also called a linear TOF spectrometer, has been successfully flown on several missions, and valuable new data have brought new insights into solar and planetary physics. Despite its benefits, the TOF–E technique also has some inherent limitations. Its M/Q resolution is limited by angular scattering and energy straggling of the incident ions in the foil, and its M resolution is severely limited by the energy resolution of the SSD, which in this application operates close to its lower detection limit.

The relative TOF uncertainty, $\Delta\tau/\tau$, of a linear TOF spectrometer is given by

$$(\Delta\tau/\tau)^2 = (\Delta\tau_e/\tau)^2 + \left(\frac{1}{2}\frac{\Delta E_{\mathrm{foil}}}{E}\right)^2 + \left(\frac{1}{2}\frac{\Delta E_{\mathrm{EA}}}{E}\right)^2 + (\Delta l/l)^2 \qquad (1)$$

which converts to the mass resolution through

$$\frac{M/Q}{\Delta(M/Q)} = \frac{1}{2}(\tau/\Delta\tau)$$

There are several contributions to the TOF uncertainty which have to be considered: the resolution of the time measuring system, $\Delta\tau_e$, the energy straggling of the ion in the foil, ΔE_{foil}, and the variability of the flight path, Δl, due to angular scattering in the foil. The resolution of the time measuring system is given by the employed electronics and the TOF dispersion of the start electrons and stop electrons. The latter can be minimized by an adequate setup. $\Delta\tau_e$ is independent of the ion energy at the entrance. Therefore, the relative error $\Delta\tau_e/\tau$ is proportional to the velocity of the particle, i.e. to the square root of the energy:

$$\Delta\tau_e/\tau = \frac{\Delta\tau_e}{l}(2E/M)^{1/2}$$

The energy straggling ΔE_{foil} is the width of the energy distribution of monoenergetic ions at the exit of the carbon foil. The usual abbreviation for this quantity is Ω, with $\Omega^2 = \langle(\Delta E - \langle\Delta E\rangle)^2\rangle$. From experimental data [8] and theoretical considerations [9], we know that the energy straggling is given by

$$\Omega/E \propto 1/(ME)^{1/2} \qquad (2)$$

The relation includes a rather complex dependence on Z_1 and Z_2 (atomic numbers of projectile and target, respectively), which is of minor interest here. The relative energy uncertainty of the energy analyzer ($\Delta E_{\mathrm{EA}}/E$), which is part of the entrance system, also has to be taken into account when evaluating the mass resolution of the entire system. It mainly depends on the chosen geometry, and for an electrostatic system it is independent of the particle energy. ($\Delta E_{\mathrm{EA}}/E$) is usually in the range 1–10%.

The angular scattering of particles passing the carbon foil causes a variation in the length of the flight path. According to Blokland et al. [10], the half width, $\psi_{1/2}$, of the angular distribution behind the foil in degrees is

$$\psi_{1/2} = 12000(Z_1{}^{3/4}S/E)$$

where Z_1 is the atomic number of the projectile, S is the area density of the carbon foil in μg cm^{-2} and E is the energy in eV. Hence the variation of the length of the flight path is

$$\Delta l/l = \left[\frac{1}{\cos(\psi_{1/2})} - 1\right]$$

Normally, this contribution is negligible; the angular scattering is only important for very low particle energies.

Fig. 2 shows the TOF resolution of a linear TOF spectrometer for the applicable energy range. The different contributions to the mass resolution, as identified in Eq. (1), are shown for an H^+ ion only. For the length of the flight path 0.2 m, and for the resolution of the time measuring system $\Delta\tau_e = 1$ ns were assumed. For the relative uncertainty (FWHM) of the energy analyzer, 1% and 10% are evaluated. This set of parameters represents the realized experimental setup, which will be described later. In an actual instrument for a space application, $(\Delta E_{EA}/E)$ would be up to 10%. For energies up to 10^5 eV, the energy straggling in the carbon foil dominates the resolution, and therefore the relative uncertainty of the TOF, $\Delta\tau/\tau$, is approximately proportional to $1/E^{1/2}$. For higher energies, the resolution is limited by the resolution of the energy analyzer and the time measuring system, since the flight time becomes shorter. For higher energies, we find $\Delta(M/Q)/(M/Q)$ proportional to $E^{1/2}$. In the center of the energy range is a minimum with optimal mass resolution $(M/Q)/\Delta(M/Q)$ where operation of the instrument is desired. Mass resolutions of actual instruments are typically ≈ 15 [11], since it is impossible to operate the instruments at the minimum of $\Delta\tau/\tau$ for all ion species. It can be seen that the mass resolution

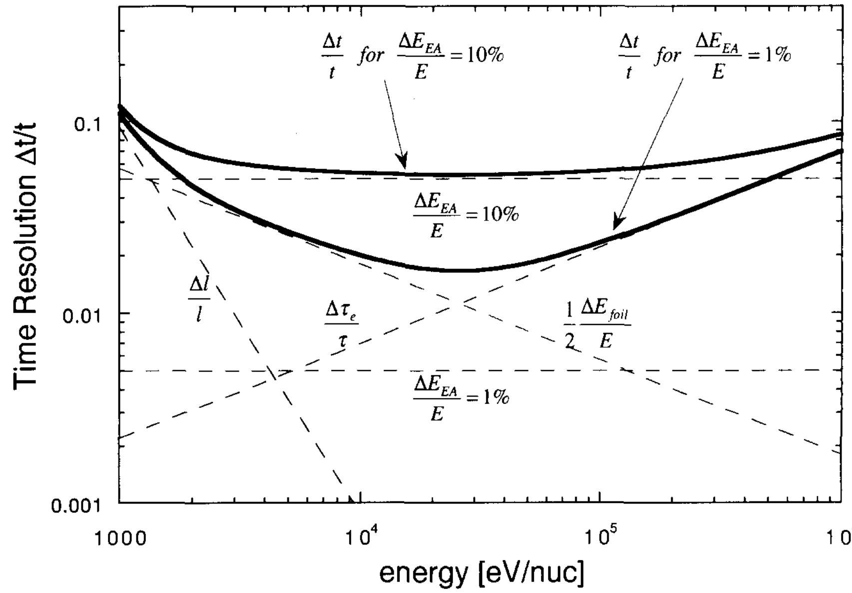

Fig. 2. Time resolution (——) of linear TOF instrument as a function of ion energy according to Eq. (1) for an instrument of 20 cm length, and resolutions of the energy analyzer of 1% and 10% for hydrogen ions. The individual contributions to the time resolution are identified (— — — —).

cannot be improved by lengthening the flight path for ion energies obtained by post-acceleration in a space instrument (currently limited to ≈ 30 kV Q).

For a TOF–E instrument, the uncertainty of the mass determination results from the limited energy resolution of SSDs. Other contributions such as the energy straggling in the foil can be neglected. An expression for the precision of the energy determination using an SSD is given by Oetliker [12]:

$$\Delta E_{\mathrm{SSD}}/E_{\mathrm{SSD}} = 1.52(M/E)^{0.92} \tag{3}$$

where M is measured in u and E is measured in keV. $\Delta E_{\mathrm{SSD}}/E_{\mathrm{SSD}}$ is essentially a result of the energy straggling of the ion in the thin conducting front layer of the SSD and of the energy loss by excitation of phonons inside the solid. In addition, it depends on the direction of propagation of the particle in the solid, because of the channeling effect. For an energy resolution of 1%, one obtains from Eq. (3) a minimal particle energy of 240 keV/nucleon. Thus the use of an SSD is only reasonable at sufficiently high particle energies. At the 10% level, 19 keV/nucleon are still necessary, which exceeds current HV technology for space applications. SSDs are suitable devices for the investigation of particle populations, which originate from such sources as solar flares and interplanetary shocks [13]. Post-acceleration of ions is applied to extend the range to lower energies, but 30 kV is currently a reasonable maximum. Therefore the resulting energies of ions in low charge states are close to the lower detection threshold of most SSDs.

2.2. Isochronous TOF instruments

With the use of a new isochronous TOF configuration, the mass resolution can be significantly improved. An isochronous TOF mass spectrometer takes advantage of the fraction of incident particles leaving the carbon foil as singly charged ions [14,15]. Within the TOF section of an isochronous instrument, the ions are reflected back to the entrance plane by a linearly increasing electrostatic field of the form $E(z) = 2wz$, which is derived from a potential of the form $\Phi(z) = wz^2$ where w is the scaling constant. The z direction is taken perpendicular to the entrance plane which is located at $z = 0$. Since the motion of the ion in the z direction is independent of the motion in the xy plane, the motion in the z direction is described by

$$\frac{\mathrm{d}^2 z}{\mathrm{d}t^2} + 2w\frac{Q}{M}z = 0$$

which corresponds to a harmonic oscillation along the z axis with a period of

$$T = \pi\left(\frac{2}{w}\frac{M}{Q}\right)^{1/2}$$

This period of oscillation is independent of the initial conditions such as initial energy or entrance angle. Therefore the TOF of an ion is only proportional to the square root of the mass to charge ratio, $(M/Q)^{1/2}$. For an ideal isochronous configuration, the resolution is only limited by the resolution of the time measuring system. The effects of the carbon foil, in particular the energy straggling and the angular scattering, cannot degrade the mass resolution any more and the mass to charge ratio of the ions can be determined accurately.

Independent of their initial charge state, the majority of particles leave the foil neutral or as singly charged ions, because of charge-exchange processes while passing the carbon foil [15,16]. The neutral particles are not deflected by the electrostatic field and leave the isochronous TOF section. Since multiply charged ions are rare at the energies considered [16], the mass per charge spectrum consists mainly of singly charged ions and thus corresponds largely to a pure mass spectrum, with little interference from doubly charged species.

2.3. Combination of linear and isochronous TOF instruments

The incoming particles that leave the start foil as neutrals are not affected by the electric field. Therefore a linear TOF channel can be added to the isochronous instrument, leading to a combined instrument with a linear and an isochronous TOF channel, which both use the same carbon foil to produce the start pulse. The ions are analyzed in the isochronous TOF channel and the particles which leave the foil as neutrals are analyzed in the linear TOF channel. If the neutrals are stopped by an SSD it is possible to obtain the charge-state distributions and the mass distribution of the investigated plasma simultaneously, the latter with a very good mass resolution.

The combination of a linear and an isochronous TOF channel leads to the following important additional application. In the carbon foil all the molecules break up into atoms. If a molecule breaks up into a neutral and a charged fragment, they can be detected simultaneously in each TOF channel and generate a double coincidence [7]. The original velocity of the molecule can be determined from the neutral fragment. Together with the E/Q information from the energy analyzer, the M/Q of the molecule can be inferred. At the same time, the mass of the charged fragment is measured with high precision. Therefore it is possible to identify simple molecules and to distinguish them from atoms or other molecules of the same mass. Results of this application are reported later in this paper.

3. Design criteria for an instrument for the measurement of three-dimensional plasma distributions

The geometric configuration of an isochronous mass spectrometer is determined by various requirements in addition to the high mass resolution. In the following section, an instrument will be described which will be able to scan the complete three-dimensional velocity distribution of ions, if operated on a spinning spacecraft. To achieve this goal, a so-called "top hat" hemispherical energy analyzer is chosen as an entrance system [17]. To fit the circular exit of the hemispherical analyzer, the TOF section has to be rotationally symmetric. The instrument is therefore called CYLMAS (CYLindrically symmetric MASs spectrometer).

The value of the electrostatic potential at any location in a charge-free field is determined by the Laplace equation. In order to fulfill the requirements stated above, the analytical expression for the potential Φ within an isochronous TOF mass spectrometer must obey the three following conditions:

(1) fulfill the Laplace equation in cylindrical coordinates

$$\Delta\Phi(r,\vartheta,z) = \left(\frac{\partial^2}{\partial z^2} + \frac{\partial^2}{\partial r^2} + \frac{1}{r}\frac{\partial}{\partial r} + \frac{1}{r^2}\frac{\partial^2}{\partial\vartheta^2}\right)\Phi(r,\vartheta,z) = 0;$$

(2) exhibit rotational symmetry $\Phi(r, v, z) = \Phi(r, z)$;

(3) allow a separation of the r and z dependences, with the z dependence being quadratic

$$\Phi(r,z) = wz^2 + \Psi(r).$$

The general solution of the Laplace equation under these three conditions has the form

$$\Phi(r,z) = a + b\log(r/R) + c[2(z/R)^2 - (r/R)^2] \tag{4}$$

where a, b, and c are free parameters, and R is a fixed geometrical scale factor. The r dependence is given by a quadratic and an additional logarithmic term. For the realization of such an instrument, it is most advantageous to choose equipotential surfaces given by Eq. (4) to shape the boundaries.

An experiment which uses a potential without the logarithmic term, i.e. of the form

$$\Phi(r, z) = a + c[2(z/R)^2 - (r/R)^2]$$

is described in Ref. [7]. It corresponds to the potential of a cylindrically symmetric quadrupole as used in an ion trap or quistor. With $c = 0$, Eq. (4) describes the logarithmic potential distribution of a cylindrical capacitor with the axis of symmetry along the z axis. In general, the potential Φ described by Eq. (4) is the sum of a quadratic and a logarithmic component. The quadratic contribution of the potential has a negative gradient in the r direction. This represents a repelling force from the center axis, and as a consequence particles are deflected outwards and may get lost. An attracting, logarithmic contribution compensates partly for this defocusing effect. Unfortunately, the logarithmic contribution decreases rapidly with increasing distance from the center axis. Such a solution was used in an instrument to analyze dust particles [18].

In the following, the optimization of parameters a, b, and c in Eq. (4) will be discussed. In Fig. 3, the important parts of a mass spectrometer using the potential given by Eq. (4) are shown. Despite the rather complex r and z dependences, only three electrodes are necessary to realize the potential: a lower, circular electrode, an upper cup, and a thin central rod. The cylindrically symmetric electrodes, the upper cup and the lower electrode are on fixed voltages. On the central rod a linearly decreasing field is generated with a special resistive coating. The radius of the detector, R, is adapted to the size of commercially available detectors. The radius of the central rod, r_s, is minimized and the potential at the footpoint of the central rod, Φ_s, is maximized within technically feasible values. Similarly, Φ_0, the voltage of the upper cup, is set at a technically feasible value. With these considerations, a

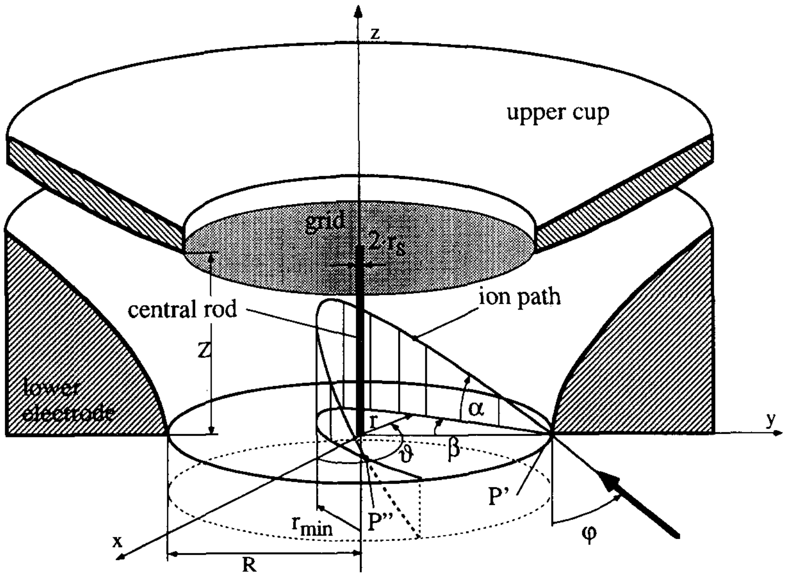

Fig. 3. Schematic cross-section through CYLMAS showing the lower electrode, the upper electrode with the grid, and the central rod. The r–ϑ–z coordinate system, the angles α and β for an ion entering the harmonic potential at point P′ and hitting the detector at P″, and the radii r_{in} and r_{min} located in the $r\vartheta$ plane are identified.

and b are defined. This leaves c open for optimization of the instrument performance. We replace c by the more convenient quantity Z/R (see Fig. 3), where R is set to the inner radius of the lower electrode. Thus Z/R is the ratio of height to diameter of the TOF section. With

$$\Phi(R,Z) = \Phi_0 = a + c[2(Z/R)^2 - 1]$$

and the above-mentioned boundary conditions, the following expression for the potential is derived:

$$\Phi(r,z) = \Phi_u + \frac{1}{2}\frac{\Phi_0 - \Phi_u}{(Z/R)^2} \times \left\{ 1 + 2(z/R)^2 - (r/R)^2 + \left[2(Z/R)^2 \frac{\Phi_s - \Phi_u}{\Phi_0 - \Phi_u} + (r_s/R)^2 - 1 \right] \times \frac{\log(r/R)}{\log(r_s/R)} \right\} \quad (5)$$

3.1. *Mass resolution of an isochronous TOF instrument*

For the mass resolution of an isochronous TOF instrument, an expression can be derived similar to that given for linear TOF instruments in Section 1. Because of the special properties of the isochronous instrument, the terms for angular scattering and energy straggling in the carbon foil can be omitted; only the uncertainty of the TOF determination remains. However, another term, $\Delta\tau_f$, has to be considered, which accounts for the non-ideal realization of the harmonic potential, mainly due to fringing fields. The expression for the mass resolution is

$$(M/\Delta M) = \tfrac{1}{2}(\tau/\Delta\tau) = \tfrac{1}{2}[(\Delta\tau_e/\tau)^2 + (\Delta\tau_f/\tau)^2]^{-1/2} \quad (6)$$

The uncertainty of the time measurement system, $\Delta\tau_e$, is a combination of the resolution of the electronics and the TOF dispersion of the start electrons. This uncertainty is constant and does not depend on the energy or mass of the particle. Therefore we can write

$$\Delta\tau_e/\tau = \frac{\Delta\tau_e}{\pi R}(cQ/M)^{1/2} = \frac{\Delta\tau_e}{\pi R(Z/R)}\left[2(\Phi_0 - \Phi_u)\frac{Q}{M}\right]^{1/2} \quad (7)$$

The limitation of the resolution due to $\Delta\tau_e$ is inversely proportional to Z/R and to the square root of the mass, because the total TOF scales with these parameters.

To estimate the influence of fringing fields on the mass resolution, the TOF of ions from the carbon foil to the detector, τ_f, can be divided into two parts: the actual isochronous TOF, τ_i, and a small additional contribution, τ_d, which corresponds to the motion in a basically field-free region $\tau_f = \tau_i + \tau_d$. The most likely place for significant deviations of the actual potential from the theoretical one is the volume in front of the detector. The variation of the TOF, τ_f, is given by $\Delta\tau_f = \Delta\tau_i + \Delta\tau_d$. For $\Delta\tau_d$, the following expression is obtained using Eq. (2) for the energy straggling in the carbon foil:

$$\Delta\tau_d \propto (M/E)^{1/2}(\Delta E_{\text{foil}}/E) \propto 1/E$$

Since the variation of the TOF in the isochronous section is zero ($\Delta\tau_i = 0$), we obtain for the total variation of the TOF $\Delta\tau_f = \Delta\tau_d \propto E^{-1}$. With the assumption $\tau_i \gg \tau_d$, the influence of the field-free space on the determination of the TOF is given by

$$\Delta\tau_f/\tau = \frac{1}{\pi R(Z/R)}\left[2(\Phi_0 - \Phi_u)\frac{Q}{M}\right]^{1/2}\frac{k}{E} \quad (8)$$

where k is a parameter which characterizes the actual realization of an instrument, e.g. fringe fields, not perfect realization of the potential, and the energy straggling in the carbon foil. Inserting Eqs. (7) and (8) into Eq. (6), we finally obtain for the mass resolution

$$M/\Delta M = \frac{\pi R(Z/R)}{2}\left[\frac{1}{2(\Phi_0 - \Phi_u)}\frac{M}{Q}\right]^{1/2} \times [\Delta\tau_e^{\,2} + (k/E)^2]^{-1/2} \qquad (9)$$

Thus the mass resolution $M/\Delta M$ is determined by three factors.

(1) $M/\Delta M$ is directly proportional to the ratio Z/R. A taller instrument results in a better mass resolution.

(2) The potential difference between the upper and lower electrodes, $\Phi_o - \Phi_u$, as well as the mass per charge ratio of an ion, determines the isochronous TOF and thereby the resolution of the instrument. The longer the TOF (the heavier the particle), the better the mass resolution $M/\Delta M$. This is another advantage of this type of instrument as it brings about high mass resolution in the mass range where it is most needed.

(3) The third factor consists of two additive terms. The first term represents the uncertainty of the time measurement system and the second term represents the imperfect realization of the electrostatic field. In order to obtain good mass resolution, both contributions must be as small as possible. A good resolution of the time measuring system does not help as long as the field realization is poor, and vice versa. The parameter k contains the effects of the energy straggling in the carbon foil (Eq. 2) and the effective dimension of the region with perturbed potential. Hence it contains instrument characteristics such as the level of perfection of the electrostatic field and the particulars of the carbon foil.

3.2. Angular acceptance

Using the laws of conservation of energy and angular momentum in the $r\vartheta$ plane, an expression for the TOF from a given entrance radius to the minimum radius in the TOF section is given by

$$T = \int_{r_{\text{in}}}^{r_{\min}} \left\{\frac{2}{M}[E_{r\vartheta} - Q\Phi(r,0)] - \frac{P^2}{M^2 r^2}\right\}^{-1/2} \mathrm{d}r$$

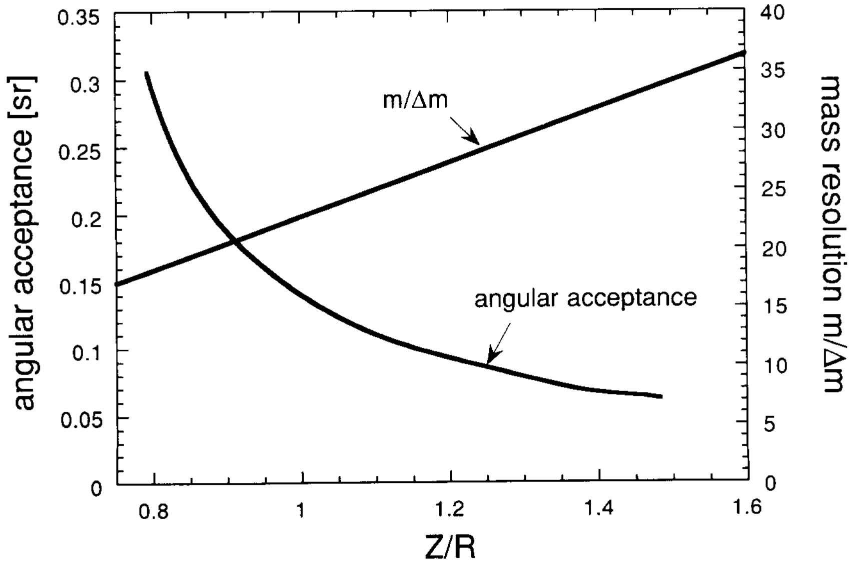

Fig. 4. Angular acceptance and mass resolution (for hydrogen) as functions of Z/R.

where r_{in} and r_{min} are defined in Fig. 3. P is the angular momentum of the ion moving in the $r\vartheta$ plane:

$$P = Mr^2 \frac{\mathrm{d}\vartheta}{\mathrm{d}t}$$

and $E_{r\vartheta}$ is the component of the total energy of the ion in the $r\vartheta$ plane:

$$E_{r\vartheta} = \frac{M}{2}\left[\left(\frac{\mathrm{d}r}{\mathrm{d}t}\right)^2 + r^2\left(\frac{\mathrm{d}\vartheta}{\mathrm{d}t}\right)^2\right] + Q\Phi(r,0)$$

Both P and $E_{r\vartheta}$ depend on the direction and energy of an ion at the point of entrance. $\Phi(r,0)$ is the electrostatic potential in the plane with $z = 0$. For successful detection of a particle, the TOF in the isochronous direction z has to be shorter than twice the time which the particle needs for the motion from r_{min} to r_{max} in the $r\vartheta$ plane (see Fig. 3). If this condition is not fulfilled above $z = 0$, the particle has a theoretical impact location with $r > R$ and hits the lower electrode instead of reaching the detector. The angular momentum of the particle is essentially determined by the entrance angle β. By varying the entrance angles α and β, the angular acceptance of the instrument can be calculated and expressed as a solid angle. The angular acceptance depends on the energy and on the instrument geometry in terms of Z/R.

The resulting angular acceptance as well as the mass resolution from the previous section are shown in Fig. 4 as a function of the parameter Z/R. As can be seen, high mass resolution has the penalty of a low angular acceptance and therefore a small geometric factor and vice versa. For practical applications a compromise has to be sought.

3.3. Numerical simulations

To determine the ion optical properties of a

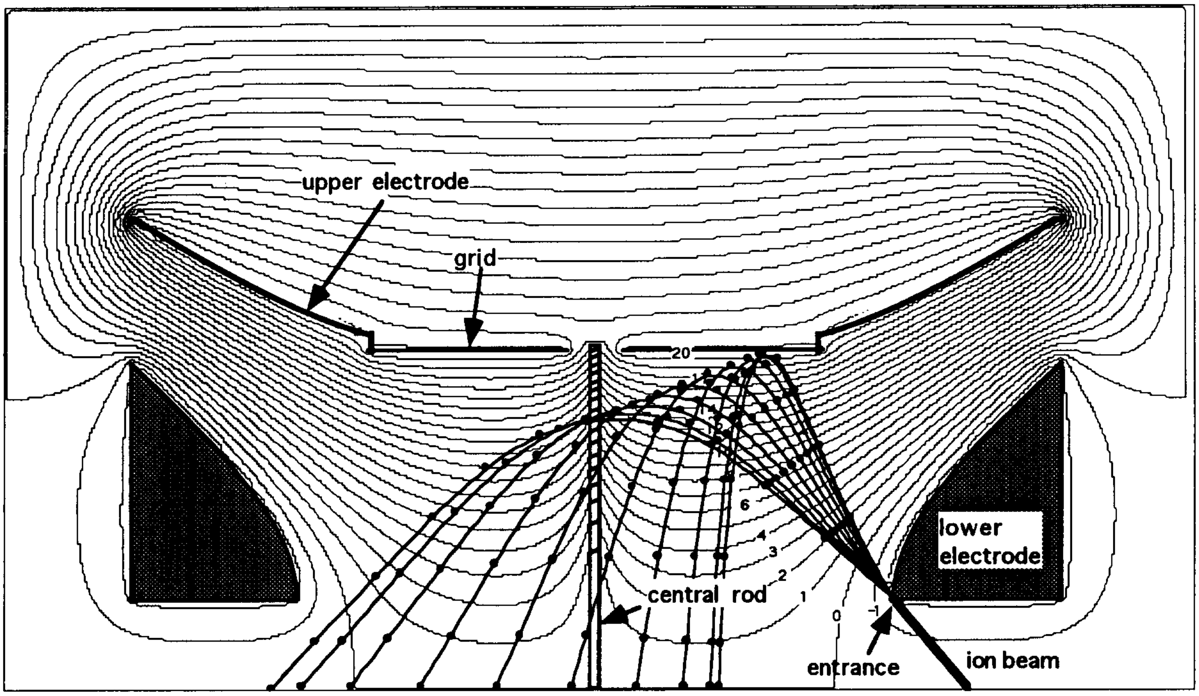

Fig. 5. Result of an ion optical simulation of the final geometry showing isocontours of the potential and ion trajectories. The points on the ion trajectories give equal time intervals to illustrate the isochronous operation of the instrument.

real electrostatic ion optical system the potential has to be calculated numerically. This allows investigations of the deviations of the electric field from the desired configuration given by Eq. (4), due to field-free space and fringing fields. Given the boundary conditions, the electrostatic potential in the empty space can be modeled with the aid of the method of finite differences. We used the successive over relaxation (SOR) method to calculate the potential, following Hageman and Young [19]. Using the resulting potential distribution, the ion trajectories can be calculated. This is accomplished with a Runge–Kutta procedure. Since the geometry of the CYLMAS instrument is rotationally symmetric, it is possible to use a two-dimensional grid which greatly reduces the computational effort in comparison to a three-dimensional calculation.

Using this numerical simulation, three parts of the instrument are optimized in terms of mass resolution: the grid, the potential distribution on the central rod, and the distance of the detector entrance plane. Fig. 5 illustrates the result of a simulation of the final geometry: the contour lines of the electrostatic potential and typical ion trajectories are shown. Time marks are given on each trajectory to illustrate the isochronous operation of the instrument.

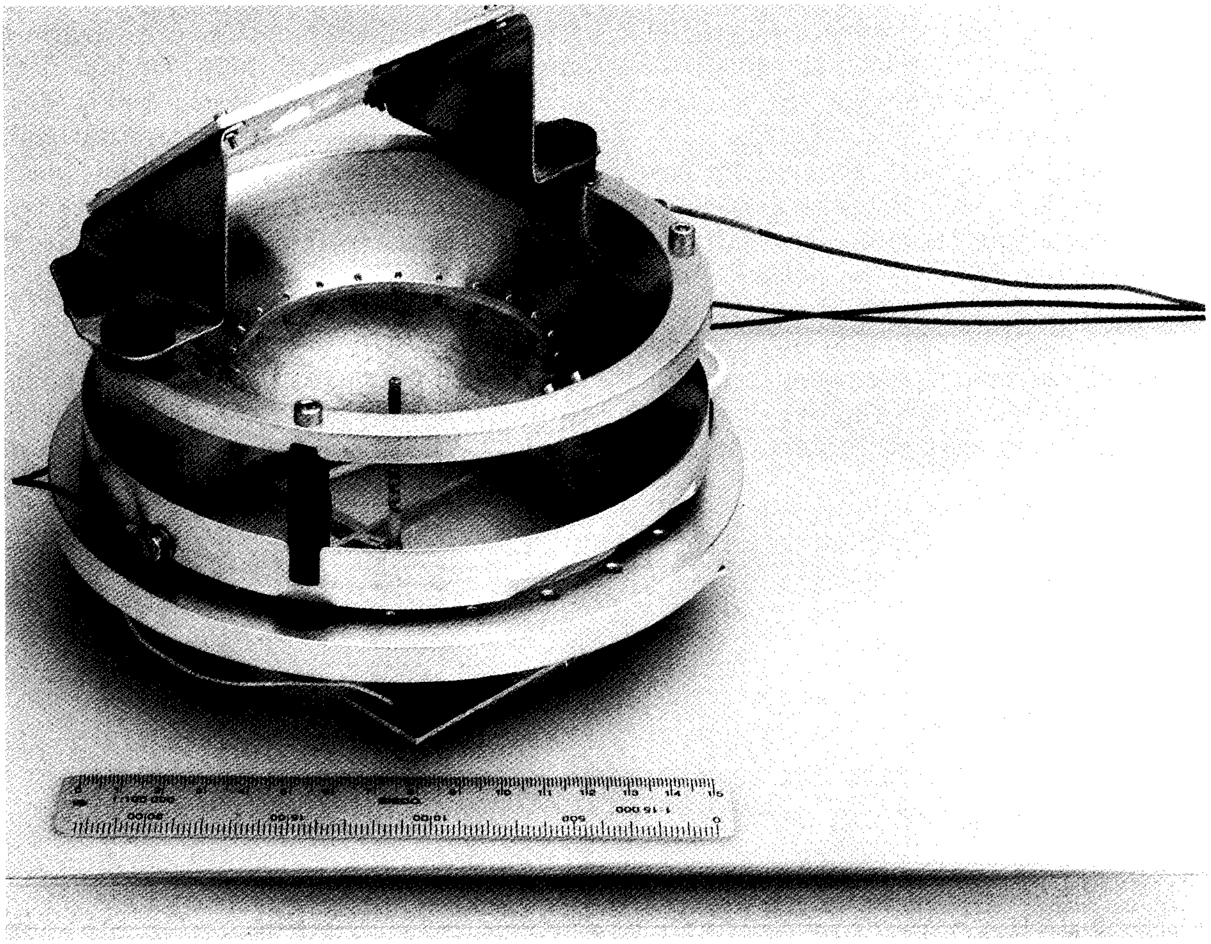

Fig. 6. Photograph of the laboratory prototype of the CYLMAS instrument. Both detectors are removed to allow a better view of the ion optical components.

4. Experimental results

4.1. Laboratory prototype

In order to demonstrate the performance of the CYLMAS instrument a laboratory prototype was built. A picture of the instrument is shown in Fig. 6. The prototype, with a single entrance location in the lower electrode and without top-hat analyzer, was tested in a calibration chamber. In Fig. 6 the particle detectors for ions, electrons, and neutral particles are removed to give a better view of the electrodes of the instrument. For both detectors, multi-channelplate detectors (MCPs) were used. They are the best choice to cover large areas and to provide short time pulses [20]. The central rod is a ceramic rod with a resistive coating chosen to produce the necessary potential conditions $\Phi(z, r_s)$ in Eq. (5).

To allow the neutral particles to pass through the upper electrode, a large part of it is realized as a grid. The ideal shape of the grid follows an isocontour of the potential from Eq. (4). It turns out that it can be approximated by a flat grid. This was confirmed with numerical simulations comparing the ideal instrument configuration with one employing a flat grid. No substantial differences between the two simulations were found. The grid was realized by wrapping a thin copper–beryllium wire (Ø 50 μm) between 24 bolts on the perimeter of the open area. A high transparency of 95% was achieved, thus minimizing the scattering of neutrals and the generation of secondary ions, which would both contribute to the background in the isochronous channel.

4.2. Isochronous TOF spectra

For the first tests of the CYLMAS prototype, a very simple ion source (Nier type) was used, providing a monoenergetic ion beam without any mass (M/Q) filtering. Thus the actual ion beam always contained a mixture of atomic and molecular ions (if a molecular gas was introduced). In Fig. 7, a typical isochronous spectrum recorded with the CYLMAS instrument is shown which was obtained using a gas mixture of CO, N_2, and O_2. The voltage settings for the instrument are $\Phi_0 = 17.5$ kV, $\Phi_u = -1.75$ kV, and $\Phi_s = 0$ V. A beam energy of 40 keV was used. With these voltage settings, only positively charged fragments from molecules breaking up in the carbon foil can be analyzed in the isochronous channel. These settings have been chosen in

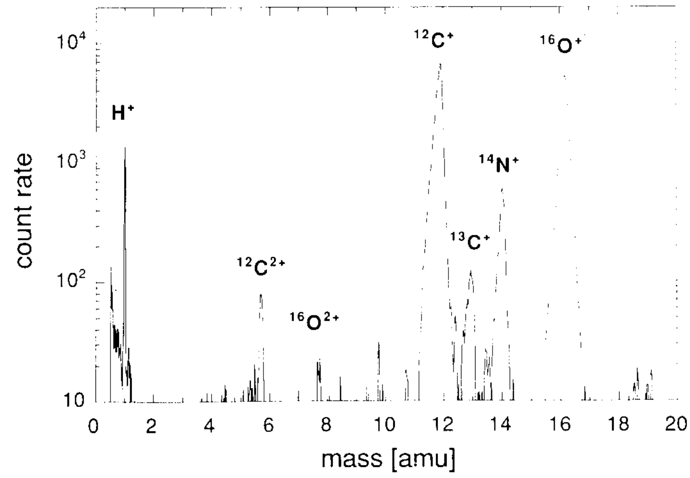

Fig. 7. Isochronous mass spectrum of the gas mixture $CO/N_2/O_2$.

order to optimize the detection of molecules (see Sections 4.5 and 4.6). The incoming atomic ions were not reflected in the instrument because their energy was too high, and they passed through the CYLMAS instrument. The major isotopes are clearly resolved as can been seen in Fig. 7. The carbon ion dominates the spectrum because carbon has a higher ionization efficiency than oxygen [16]. On a logarithmic scale, contributions from rare components become visible: $^{13}C^{+}$ as well as the doubly ionized species $^{12}C^{2+}$ and $^{16}O^{2+}$ can be identified. The spectrum shown in Fig. 7 is smoothed (three-point-interval smoothing) and the background is subtracted after fitting it with a polynomial.

4.3. Mass resolution

Based on measurements with various gas mixtures and beam energies, the dependence of the mass resolution on the mass was investigated. For hydrogen, a mass resolution of 17 and for the heavier atoms like C, N and O a mass resolution of approximately 67 was achieved. Fig. 8 shows a comparison between the results from several measurements and Eq. (9). Since these measurements were performed at different beam energies, different mass resolutions are obtained. From Eq. (9) we expect a dependence $M/\Delta M \propto E^{1/2}$. With $k = 1.58 \times 10^{-4}$ eV, all measurements are reproduced well by Eq. (9) after taking into account the energy loss in the carbon foil. The two dotted lines in Fig. 8 represent the mass resolution according to Eq. (9) for ions with the highest and lowest beam energies. All data points are consistent with Eq. (9). The value of $k = 1.58 \times 10^{-4}$ eV corresponds to a length of the perturbed field of 15 mm, and a width of the TOF peak of ≈ 2 ns. The latter value has been observed in the recorded spectra, and the length of the perturbed field region matches with the gap between the lower electrode and the detector. Thus, the ansatz for the mass resolution is indeed justified. The Z_1 and Z_2 dependences of the energy straggling (Eq. (2)) is not included in Eq. (9), and could be the reason for the straggling of the data points around the calculated mass resolution.

The non-ideal field in front of the detector is the main reason for the limitation in mass resolution. Unfortunately, there is no simple remedy for this limitation, since the entrance

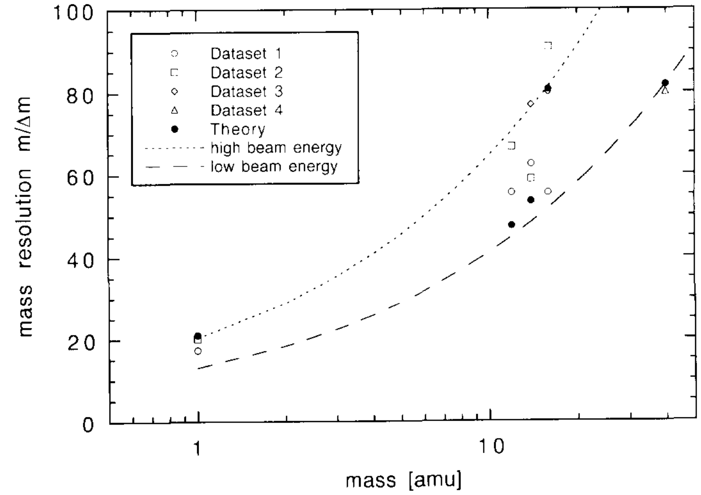

Fig. 8. Comparison of the measured mass resolution for different masses with the theoretical mass resolution given by Eq. (9). The different data sets are recorded with different beam energies (30–40 keV). Theoretical values are given for the lowest (————) and highest (···) beam energy used.

of the detector is a conducting surface and thus defines an equipotential plane at a location where a potential gradient would be required. As mentioned above, the settings of the CYLMAS instrument for these measurements were optimized for the detection of molecules. If the CYLMAS instrument parameters are optimized for atomic ions, further improvement of the mass resolution is observed (Fig. 9).

4.4. Determination of isotopic ratios

The mass resolution of the CYLMAS instrument is sufficient to resolve isotopes and to determine the natural abundance ratios of the isotopes $^{12}C/^{13}C$, $^{14}N/^{15}N$ and $^{16}O/^{18}O$ (see Fig. 10). The obtained spectra can be analyzed accordingly and the results are compared to terrestrial values. For the $^{12}C/^{13}C$ ratio we obtain 1.3% (1.1%), for the $^{14}N/^{15}N$ ratio we obtain 0.38% (0.37%), and for the $^{16}O/^{18}O$ ratio we obtain 0.24% (0.20%), with the terrestrial values given in parentheses. The analysis of the spectra involves smoothing of the data, background fitting by a polynomial, subtraction of the background, and integration of the resulting peak over the pertaining intervals. The resulting error bars of these measurements are still substantial. Significant improvement can be expected, however, with longer data collection intervals. The intention of these measurements was primarily to show that the isochronous instrument is in principle able to determine isotopic abundance ratios. Obviously, the suppression of false coincidences, caused by particle scattering and electronic noise, is important. In our case, extending the measuring period would help to significantly reduce the error bars.

4.5. Spectra of H_2 molecules

The two TOF channels, the isochronous and the neutral channel, use the same carbon foil to produce a start pulse. If only those TOF measurements are considered when a signal is registered in both channels simultaneously, i.e. when signals which belong to the same start pulse are detected on both stop detectors, it

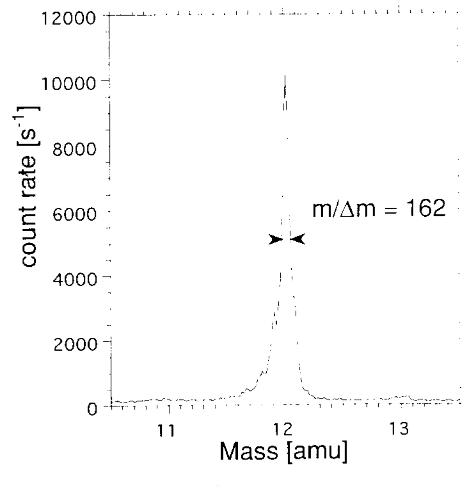

Fig. 9. Mass resolution for ^{12}C with CYLMAS optimized for atomic ions.

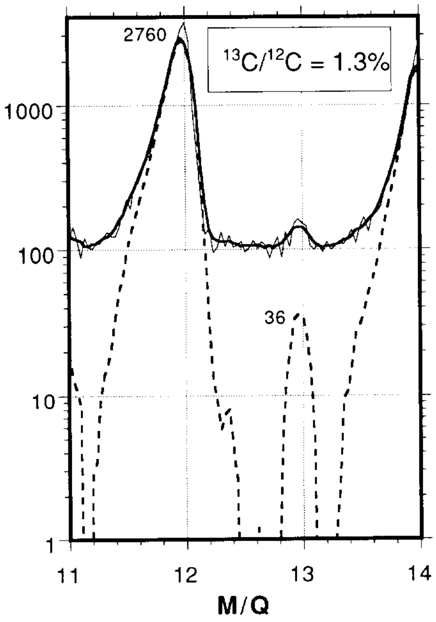

Fig. 10. Sections of the mass spectrum shown for the determination of isotope ratios for C, N, and O.

is possible to identify molecules. During passage through the carbon foil the molecule has to form a positively charged and a neutral fragment. The positive ion fragment is detected in the isochronous TOF channel, while the neutral fragment is detected in the linear TOF channel. The neutral fragment can be used to determine the velocity of the original molecule. Together with the *E/Q* information from the energy analyzer, or in our case the voltage of the ion accelerator, the total mass of the molecule can be derived. The mass of the charged fragment is measured in the isochronous channel at the same time. This information suffices to identify simple molecules.

The principle of operation and the possibilities of this method are demonstrated with measurements of the H_2 molecule. The simultaneously measured flight times in the isochronous channel and in the linear channel form pairs of numbers which can be plotted as a two-dimensional histogram. Fig. 11 shows such a two-dimensional representation of the coincident flight times for an ion beam consisting of H^+ and H_2^+ ions. Practically all ions have the same TOF in the isochronous channel, which corresponds to the TOF of an H^+ fragment from the incoming H_2^+ molecule. The TOF in the neutral channel is also approximately the same for all events in this channel and is attributed to the neutral H

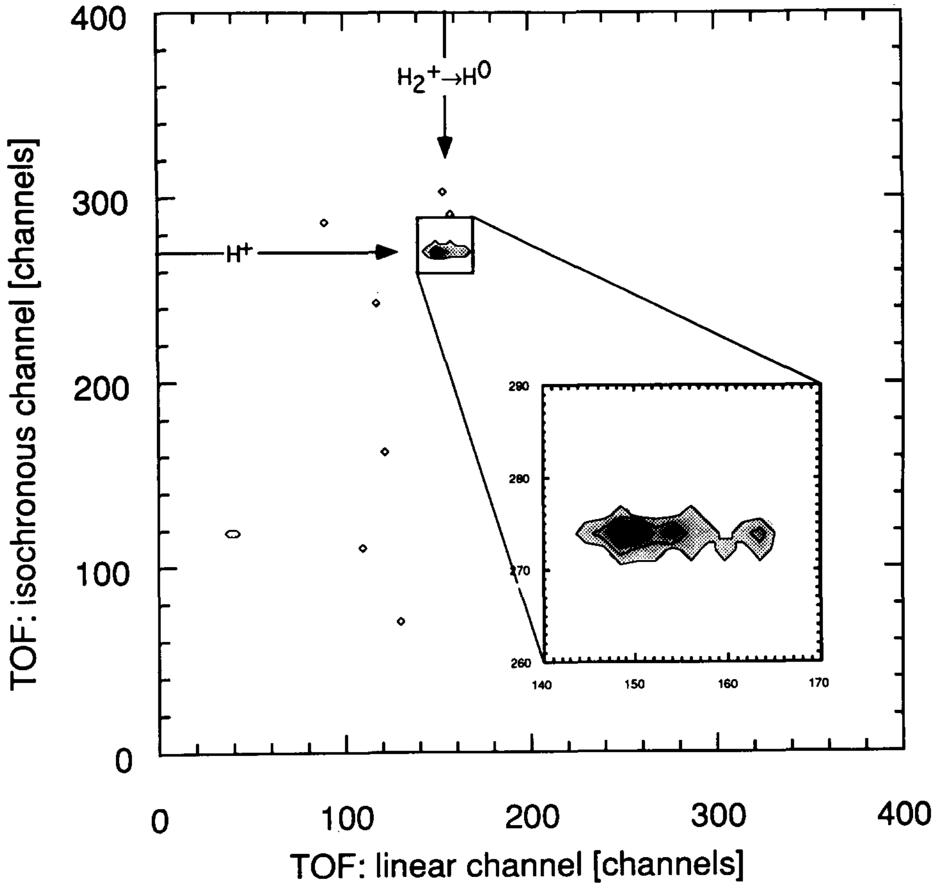

Fig. 11. Identification of the H_2 molecule with CYLMAS using the isochronous and the neutral channel simultaneously for particle detection.

fragment originating from the incoming H_2^+ molecule. The few other dispersed points are caused by accidental coincidences and signals from scattered particles. Fig. 12 shows a histogram of flight times in the neutral channel for all events and for a subset of coincident events. Two additional peaks are visible in the full TOF spectrum (all events) when compared with the coincidence spectrum of the neutral channel. These two additional peaks result from hydrogen ions which lost their bonding partner in the ion source and entered the instrument as protons. In the acceleration region of the ion source they obtain a higher velocity than the H_2 molecules, which results in a shorter TOF. Since the H^+ ion cannot produce double coincidences, the two peaks for neutral and singly charged hydrogen are not visible in the histogram of Fig. 12. This demonstrates that an unambiguous identification of H_2 molecules is possible.

4.6. Spectra of other diatomic molecules

The measurement reported in Section 3.4 can be applied to any other diatomic molecule. In that case, the identification of the second fragment in the neutral channel becomes more difficult owing to the limited mass resolution of the neutral channel (see Section 2.1). In Fig. 13, the two-dimensional histogram for the measurement of the gas mixture consisting of CO, N_2 and O_2 is shown. The resolution in the isochronous channel is more than sufficient and allows for a very accurate determination of the mass of

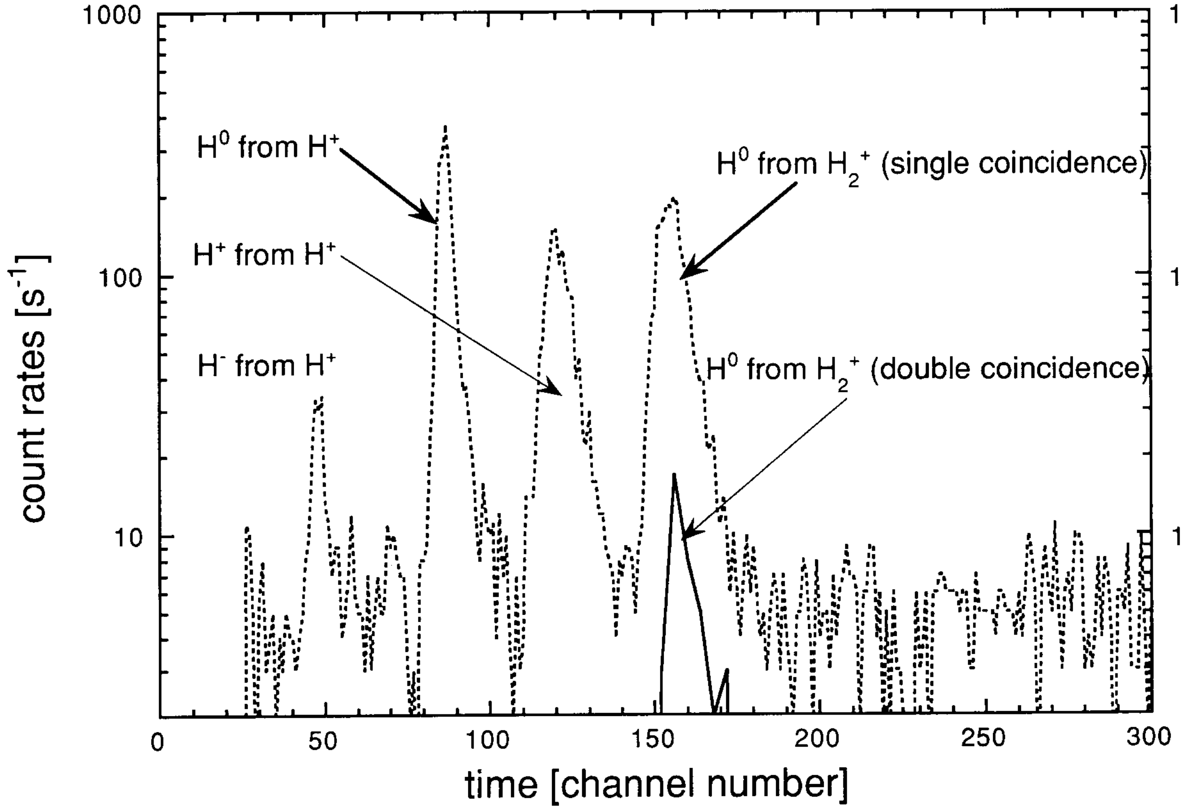

Fig. 12. Histogram of flight times in the neutral channel for coincidence events (neutral and isochronous channel simultaneously) as compared to all events.

the charged fragment. The spectrum in the neutral channel is somewhat harder to interpret because of the large energy spread of the particles after their passage through the carbon foil. The molecules no longer appear as single spots in Fig. 13, but as elongated strips along the x axis (which represents the TOF in the neutral channel). However, after a more careful deconvolution of the data it is possible to identify all molecular ions, CO, N_2, and O_2, which entered the instrument [21]. The TOF distribution of the particles measured in the neutral channel, which are in coincidence with the detection of a C^+ ion in the isochronous channel, is shown in Fig. 14 together with the TOF distribution of all events in the neutral channel (···). Two peaks can be clearly identified, one for O^- and one for O^0. Both are fragments of singly charged CO molecules. Two additional peaks are possibly due to sputtering of C^+ from the carbon foil with O^+ and O^{2+} projectiles.

The limitations in resolution of the neutral channel can be overcome if a second isochronous channel is used instead of the neutral channel. In this mode, the incoming molecule has to break up into two charged fragments. This measurement is accomplished by splitting the anode of the detector in the isochronous channel into several segments whose signals are read out independently. For the following measurement two different segments of the detector have been used. The result is shown in Fig. 15. CO and N_2 molecules can be clearly identified without further data manipulation. The diagonal line with coincidence events, visible for short flight times, is due to cross-talk between the two detector segments. This can be eliminated with an appropriate suppression of scattered particles on the MCP front side, by reducing the ion feedback effect, and improved shielding of the anode segments. The two segments which were used to detect the fragments are

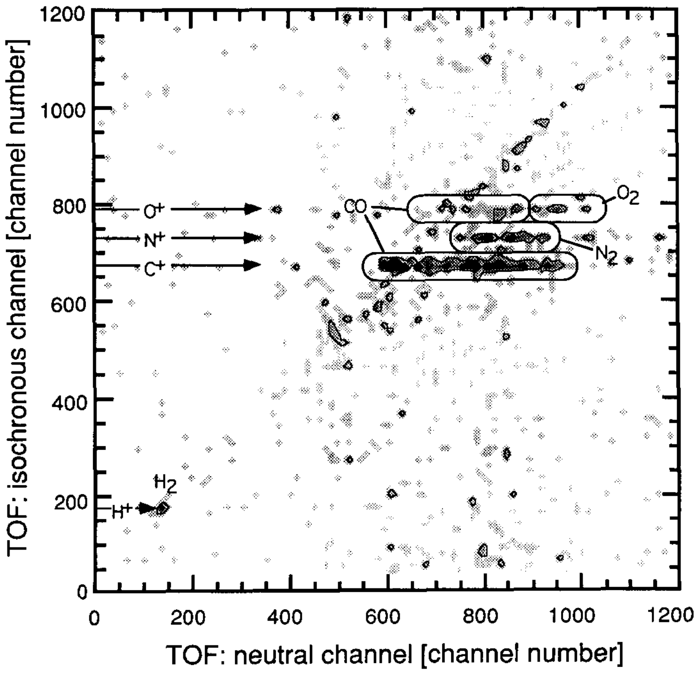

Fig. 13. Identification of CO, N_2, and O_2 molecules with CYLMAS using the isochronous and the neutral channel simultaneously for particle detection.

located at different distances from the entrance location of the ion beam. The most prominent peak in Fig. 15 corresponds to events when C^+ is registered on the segment which is further away from the carbon foil than the segment which registers O^+. This implies that the O^+ ion has a shorter flight path than the C^+ ion, and that it therefore entered with less energy. The segmented anode leads to a low detection efficiency for molecules in this mode. In the future, these measurements will be performed with a time measuring system which can accept multiple stop events in one channel and therefore the entire detector area can be used. This is also a natural remedy for the cross-talk.

It is evident from the presented results that the technique of multiple coincidences allows the determination of molecules by directly measuring the masses of their constituents with high resolution. Molecules having the same mass number but consisting of different atoms can be clearly distinguished, and isotopic abundances can also be determined. In particular, the identification of CO and N_2 has been demonstrated, which is of interest for the mass spectrometry of space plasmas. This opens up new perspectives in the construction of versatile high resolution, space-borne mass spectrometers and will lead to interesting applications in space research.

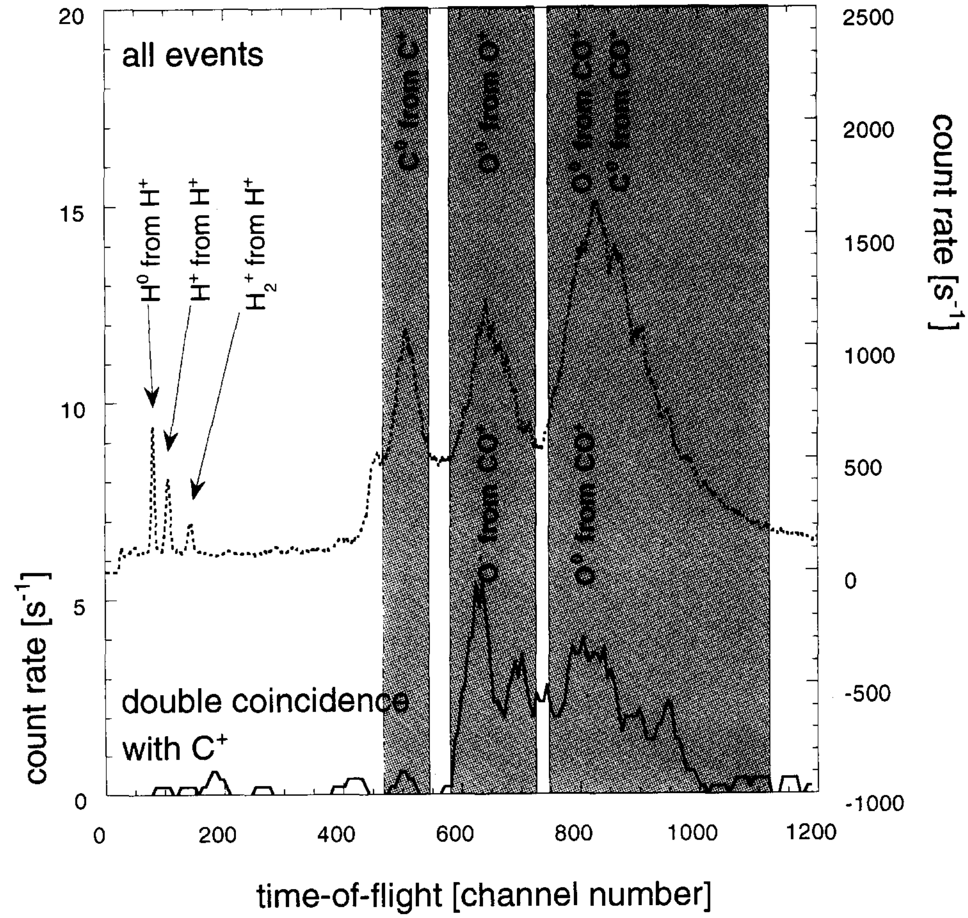

Fig. 14. TOF histograms in the neutral channel either measured in coincidence with C^+ ions detected in the isochronous channel (——) or for all events (···).

5. Further improvements

There is still room for improvement of the instrument. The measurements show where changes in the design of such an instrument are necessary. The most important goal is the reduction of background. The importance of background reduction has been addressed in detail in a recent paper [22]. The major portion of the background originates from scattering of particles from electrodes. Many particles emerging from the carbon foil cannot be detected in the isochronous channel because they are not positively charged and cannot be deflected in the electrostatic field. After scattering from electrodes these particles can produce false coincidences. The measures to reduce the background from scattered particles can be divided into two groups, as follows.

(1) The comparably abundant neutrals should not hit surfaces which form the boundary of the TOF volume. Scattering and charging effects produce ions and electrons which generate signals on the isochronous stop detector in coincidence with start pulses. Therefore the neutrals must leave the isochronous TOF section unimpeded. This is achieved with an open geometry. The present version of the upper electrode of the CYLMAS instrument already consists mostly of a grid. However, neutrals having moved outside the TOF section should not undergo any process which releases electrons, since electrons could be accelerated back into the instrument through the highly positive upper electrode and thereby cause false coincidences.

(2) The ions should be detected with high efficiency. Every part of the instrument must

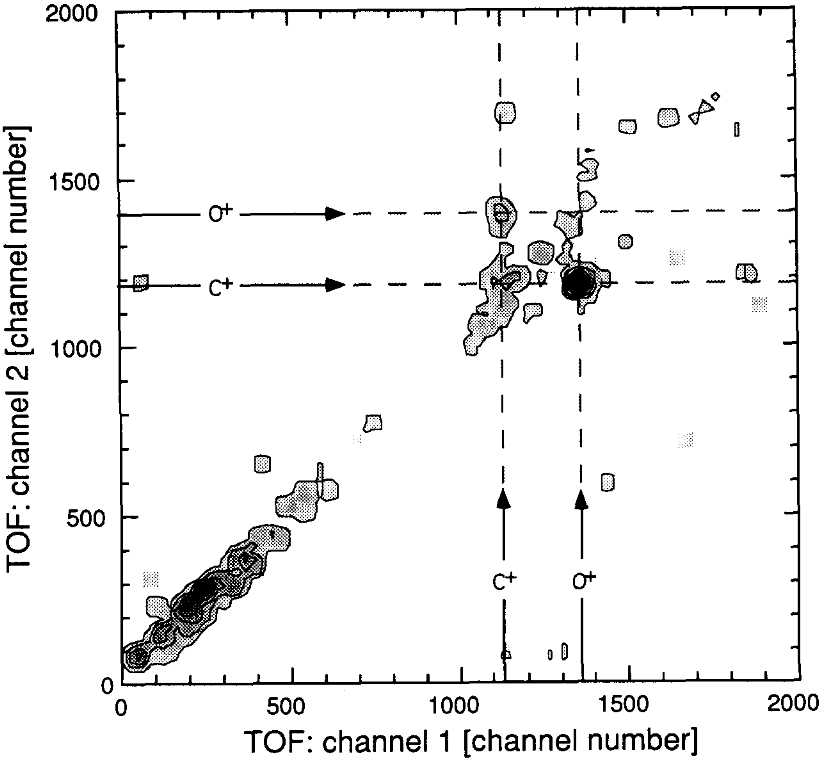

Fig. 15. Identification of CO molecules with CYLMAS using two separate segments of the detector of the isochronous channel for simultaneous particle detection.

be designed and optimized accordingly. The aim is to maximize the yield of start pulses from ions. After passing the foil, ions should hit the detector in the ground plane, rather than other electrodes, and generate stop pulses with high efficiency. For example, the optimization of the electrostatic field, including a logarithmic term to focus the ions inside the spectrometer, is an important step to reduce the background of false coincidences and to improve the detection efficiency of ions.

Acknowledgments

The authors are grateful to J. Fischer, H. Hofstetter, and R. Liniger from the University of Bern for their contributions in the areas of design, fabrication and electronics, respectively, to R. Burkhalter and H. Schwab from the Ingenieurschule Biel, Switzerland, for their help in design and construction, and to K. Crocker, M. Granoft, and E. Kistler from the University of New Hampshire for their help in the design and fabrication of the MCP detector of the isochronous channel. The work at the University of Bern was supported by the Swiss National Science Foundation, and the work at the University of New Hampshire was partly funded under the NASA Contracts #NAS 5-31283 and #NAS 5-30613.

References

[1] G. Gloeckler and K.C. Hsieh, Nucl. Instrum. Methods, 165 (1979) 537.
[2] E. Möbius, G. Gloeckler, D. Hovestadt, F.M. Ipavich, B. Klecker, M. Scholer, H. Arbinger, H. Höfner, E. Künneth, P. Laeverenz, A. Luhn, E.O. Tums and H. Waldleben, IEEE Trans. Geosci. Remote Sensing, GE-23(3) (1985) 274.
[3] D. Hovestadt, J. Geiss, G. Gloeckler, E. Möbius, P. Bochsler, F. Gliem, F.M. Ipavich, B. Wilken, W.I. Axford, H. Balsiger, A. Bürgi, M. Coplan, H. Dinse, A.B. Galvin, K.I. Gringauz, H. Grünwaldt, K.C. Hsieh, B. Klecker, M.A. Lee, G.G. Managadze, E. Marsch, M. Neugebauer, W. Rieck, M. Scholer and W. Stüdemann, ESA SP-1104 (1989) 69.
[4] R. v. Steiger, J. Geiss, G. Gloeckler, H. Balsiger, A.B. Galvin, U. Mall and B. Wilken, in Goslar Proceedings, Pergamon, Germany, 1991.
[5] D.J. McComas and J.E. Nordholt, Rev. Sci. Instrum., 61 (1990) 3095.
[6] D.C. Hamilton, G. Gloeckler, F.M. Ipavich, R.A. Lundgren, R.B. Sheldon and D. Hovestadt, Rev. Sci. Instrum., 61 (1990) 3104.
[7] E. Möbius, P. Bochsler, A.G. Ghielmetti and D.C. Hamilton, Rev. Sci. Instrum., 61 (1990) 3609.
[8a] J.C. Eckardt, Phys. Rev. A, 18 (1978) 426.
[8b] P. Beiersdorf, A.L. Roquemore and R. Kaita, Rev. Sci. Instrum., 58 (1987) 2092.
[9] J.C. Ashley, A. Gras-Marti and P.M. Echenique, Phys. Rev. A, 34 (1986) 2495.
[10] A.A.E. v. Blokland, T.W.M. Grimbergen and H.W. v. d. Ven, Rev. Sci. Instrum., 63 (1992) 1978.
[11] G. Gloeckler, J. Geiss, H. Balsiger, P. Bedini, J.C. Cain, J. Fischer, L.A. Fisk, A.B. Galvin, F. Gliem, D.C. Hamilton, J.V. Hollweg, F.M. Ipavich, R. Joos, S. Livi, R. Lundgren, U. Mall, J.F. McKenzie, K.W. Ogilvie, F. Ottens, W. Rieck, E.O. Tums, R. v. Steiger, W. Weiss and B. Wilken, Astron. Astrophys. Suppl. Ser., 92 (1992) 267.
[12] M. Oetliker, CTOF, A solar wind time of flight mass spectrometer with high charge resolution: numerical simulations and calibrations, Ph.D. Thesis, Universität Bern, Bern, Switzerland, 1993.
[13] G.L. Mason, D.C. Hamilton, P.H. Walpole, K.F. Heuerman, T.L. James, M.H. Lennard and J.E. Mazur, IEEE Trans. Geosci. Remote Sensing, 31 (1993) 549–556.
[14] P. Hvelplund, E. Lægsgård, J.Ø. Olsen and E.H. Pedersen, Nucl. Instrum. Methods, 90 (1970) 315.
[15] M. Gonin, A. Bürgi, M. Oetliker and P. Bochsler, ESA SP-348, (1992) 381.
[16] A. Bürgi, M. Oetliker, P. Bochsler, J. Geiss and M.A. Coplan, J. Appl. Phys., 68 (1990) 2547.
[17] M.J. Sablik, D. Golimowski, J.R. Sharber and J.D. Winnigham, Rev. Sci. Instrum., 59 (1988) 146.
[18] V.P. Ivanov, A.A. Makarov and A.A. Sysoey, in Proc. 4th Int. Seminar on Manufacturing of Scientific Space Instrumentation, Frunse, USSR, Academy of Sciences of the USSR, Space Research Institute, 1989.
[19] L.A. Hageman and D.M. Young, Computer Science and Applied Mathematics, Academic Press, New York, 1981.
[20] P. Wurz and L. Gubler, Rev. Sci. Instrum., 65 (1994) 871.
[21] L. Gubler, Isochrone Flugzeit-Massenspektrometer für den Einsatz im Weltraum, Ph.D. Thesis, University of Bern, Switzerland, 1994.
[22] P. Bochsler and E. Möbius, ESA SP-1157, (1994) 43.